

Structure of the defect perovskite $\text{Ce}_{1/3}\text{NbO}_3$: a redetermination by electron and neutron powder diffraction

C. Bridges,* J. E. Greedan and J. Barbier

Brockhouse Institute for Materials Research,
McMaster University, Hamilton, Ontario,
Canada L8S 4M1

Correspondence e-mail: greedan@mcmaster.ca

The crystal structure of the defect perovskite $\text{Ce}_{1/3}\text{NbO}_3$, cerium niobium oxide, has been re-examined by neutron powder and electron diffraction. The results of a powder neutron Rietveld refinement indicate that the structure is monoclinic: space group $P2/m$ with $Z = 4$, $a = 5.5267(3)$, $b = 7.8824(2)$, $c = 5.5245(3)$ Å, $\beta = 90.294(1)^\circ$, $V = 240.67(2)$ Å³ at 298 K with $\chi^2 = 2.570$. Previous reports have described the $\text{Ce}_{1/3}\text{NbO}_3$ structure in a smaller ($V/2$) orthorhombic cell based solely upon X-ray powder diffraction data. The presence of weak reflections in the electron diffraction pattern provides conclusive evidence for a monoclinic superstructure of the orthorhombic cell. While these superlattice reflections are barely detectable with X-ray radiation, they are clearly visible in the neutron diffraction experiments. The superlattice reflections are shown to arise from a tilting of the NbO_6 octahedra which results in the reduction of symmetry from orthorhombic to monoclinic. It is also found that the Ce^{3+} and Nb^{5+} cations are displaced from the centres of their respective polyhedra to accommodate the bond-valence requirements of the crystal structure. It is likely that distortions of this type are present in other $\text{Ln}_{1/3}\text{NbO}_3$ and $\text{Ln}_{1/3}\text{TaO}_3$ defect perovskites.

Received 7 July 1999

Accepted 12 October 1999

1. Introduction

As a class of materials, perovskite-based compounds have attracted a wide range of industrial and academic interest. The cation-deficient perovskite oxides with the general formula $\text{Ln}_{1/3}\text{NbO}_3$ ($\text{Ln} = \text{La}, \text{Ce}, \text{Pr}$ or Nd) have been investigated by Orgaz & Huanosta (1992) and Abakumov *et al.* (1995) for their electrical properties. Assignment of the crystal structure in these studies has been based upon a model in the $Pmnm$ space group initially proposed by Iyer & Smith (1967) from X-ray diffraction data. Two polymorphs of $\text{Ln}_{1/3}\text{NbO}_3$ are presently known. The high-temperature polymorphs, which corresponds to the Iyer & Smith (1967) model, have been referred to as the orthorhombic β modification of $\text{Ln}_{1/3}\text{NbO}_3$. The structures of the low-temperature α - $\text{Ln}_{1/3}\text{NbO}_3$ polymorphs, which have been prepared under hydrothermal conditions, have been determined in the monoclinic space group $P2_1/c$ by Torardi *et al.* (1985).

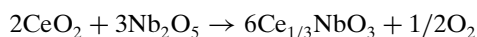
It is well known that in the presence of heavy atoms, small displacements of the oxygen positions can be difficult to detect by X-ray diffraction. For this type of problem neutron diffraction, with its relatively large sensitivity to oxygen scattering, has an advantage.

The work of Iyer & Smith (1967) involved a combination of single crystal and powder data for the La, Pr and Nd compounds, although only powder data was analysed for $\text{Ce}_{1/3}\text{NbO}_3$. More recent studies have used only X-ray powder diffraction data to investigate the structures of this series. The

present work has re-examined the high-temperature form of $\text{Ce}_{1/3}\text{NbO}_3$ using both neutron powder and electron diffraction data. These data indicate that the compound is best described by the monoclinic space group $P2/m$ rather than the orthorhombic $Pmmm$.

2. Synthesis

Samples were prepared through solid-state reaction of CeO_2 (99.99%, Research Chemicals) and Nb_2O_5 (99.9+%, Alfa Aesar). Stoichiometric amounts were mixed under acetone in an agate mortar. Pellets of the starting materials were reacted in air at 1473 K for 60 h. This produced $\text{Ce}_{1/3}\text{NbO}_3$ according to the reaction below.



The product was a light brown powder which was determined to be phase pure by X-ray powder diffraction.

3. Data collection

3.1. X-ray powder diffraction

Samples were analysed using a Guinier–Hägg camera (IRDAB Model XDC700) with $\text{Cu } K\alpha_1$ radiation and a silicon internal standard. The positions and intensities of the reflections were measured using a KEJ Instruments model LS20 line scanner to produce a digitized data file. Cell refinements and indexing were carried out with the program *LSUDF*.

3.2. Transmission electron microscopy

A Philips CM-12 microscope operating at 120 keV was used to obtain electron diffraction patterns. The product was examined as a finely ground powder deposited onto holey carbon films supported by copper grids.

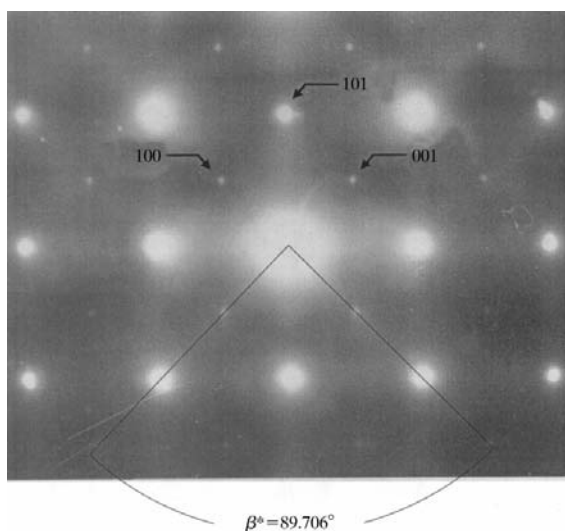


Figure 1
An electron diffraction pattern of the [010] zone of the monoclinic unit cell [$a = 5.5266$ (3), $b = 7.8828$ (2), $c = 5.5251$ (3) Å, $\beta = 90.294$ (1)°] displaying the weak superstructure reflections.

Table 1
Experimental details.

Crystal data	
Chemical formula	$\text{Ce}_{1/3}\text{NbO}_3$
Chemical formula weight	187.61
Cell setting	Monoclinic
Space group	$P2/m$
a (Å)	5.5267 (3)
b (Å)	7.8824 (2)
c (Å)	5.5245 (3)
β (°)	90.294 (1)
V (Å ³)	240.67 (2)
Z	4
Radiation type	Neutron
Temperature (K)	298
Density (Mg m ⁻³)	5.173
Specimen preparation temperature (K)	1200
Colour	Brown
Data collection	
Diffractometer	SEPD
Data collection method	Time-of-flight
Instrument location	IPNS, Argonne National Laboratories
Specimen mounting	Vanadium can
Specimen mounted	Transmission mode
Absorption correction	Debye–Scherrer (Hewat, 1979)
Special details	Reference for the calibration of SEPD data: Jorgensen <i>et al.</i> (1989)
Refinement	
R_p	0.035
R_{wp}	0.057
S	1.60
Profile function	Convolution of exponentials and a Gaussian (Von Dreele <i>et al.</i> , 1982)
Excluded region(s) (Å)	0.0000–0.5366
No. of parameters used	60
$(\Delta/\sigma)_{\text{max}}$	0.01
Source of atomic scattering factors	<i>International Tables for Crystallography</i> (1992, Vol. C)
Computer programs	
Structure refinement	GSAS (Larson & Von Dreele, 1986)

3.3. Neutron powder diffraction data

Data were collected at 298 K on the SEPD diffractometer at the Intense Pulsed Neutron Source (IPNS) at Argonne National Laboratory. Analysis of the time-of-flight neutron powder diffraction data was performed using the GSAS Rietveld refinement software package (Larson & Von Dreele, 1986).

4. Results

4.1. Analysis of X-ray powder and electron diffraction data

As previously discussed, X-ray single crystal and powder diffraction data are consistent with an orthorhombic structure described in the space group $Pmmm$ (Abakumov *et al.*, 1995) with unit-cell parameters $a = 3.899$ (1), $b = 3.917$ (1) and $c = 7.881$ (2) Å. Guinier powder diffraction data for $\text{Ce}_{1/3}\text{NbO}_3$ collected in our laboratory can also be indexed on this unit

cell, with cell parameters $a = 3.895$ (1), $b = 7.876$ (2) and $c = 3.915$ (1) Å. However, transmission electron microscopy (TEM) of the same sample reveals a deviation from 90° for the β angle of the orthorhombic cell (for the cell setting in which b is the long axis). Moreover, weak superstructure reflections are present in a [101] zone-axis pattern which can only be indexed on a $(2)^{1/2}a \times b \times (2)^{1/2}c$ supercell (b is the long axis) of the $Pmmm$ unit cell (Fig. 1). The [100] and [001] reflections of this monoclinic cell are extremely weak, indicating that the heavy atom positions are close to those expected for the $Pmmm$ cell and that the intensity of these reflections origi-

nates largely from the O atoms. A neutron diffraction study was therefore carried out in order to determine accurate coordinates for all atoms.

4.2. Analysis of neutron powder diffraction data

The starting model for refinement of the data was based upon the $\text{La}_{0.38}\text{NbO}_3$ structure solution of Abakumov *et al.* (1995) in $Pmmm$. The results of a refinement in $Pmmm$ are shown in Fig. 2(a). All positional parameters and isotropic temperature factors were varied, although simultaneous refinement of all parameters was not possible. This resulted in poor refinement statistics, *viz.* $R_p = 0.1291$, $R_{wp} = 0.1966$ and $\chi^2 = 30.16$ for 15 parameters. The difference plot also shows poor agreement between the calculated and observed profiles with several reflections not accounted for by the orthorhombic model (*e.g.* the two peaks near 2.35 Å in the inset of Fig. 2a).

An improved model was derived by a transformation from $Pmmm$ to the larger $(2)^{1/2}a \times b \times (2)^{1/2}c$ supercell. In addition, a distortion to monoclinic symmetry was required to index all the observed reflections. This distortion and the need for a larger unit cell agree with the results of the TEM data. The monoclinic cell is twice the size of the $Pmmm$ cell and a comparison between the two cell settings is given in Fig. 3. Examination did not reveal any systematic absences, consistent with three monoclinic space groups: $P2$, Pm and $P2/m$. The first model tested was $P2/m$, as it is a maximal non-isomorphic subgroup of $Pmmm$ and the only centrosymmetric space group of the three possibilities. The higher symmetry in the atomic positions was broken by tilting the NbO_6 octahedra in the manner expected for such a perovskite (as described in the *Discussion*). All positional parameters and isotropic temperature factors were refined. Other variable parameters included an overall scale factor, a power series with four terms to describe the background, an absorption coefficient and six profile parameters. In the final stages of refinement all positional and atomic displacement parameters were varied simultaneously, but the absorption coefficient was held constant.

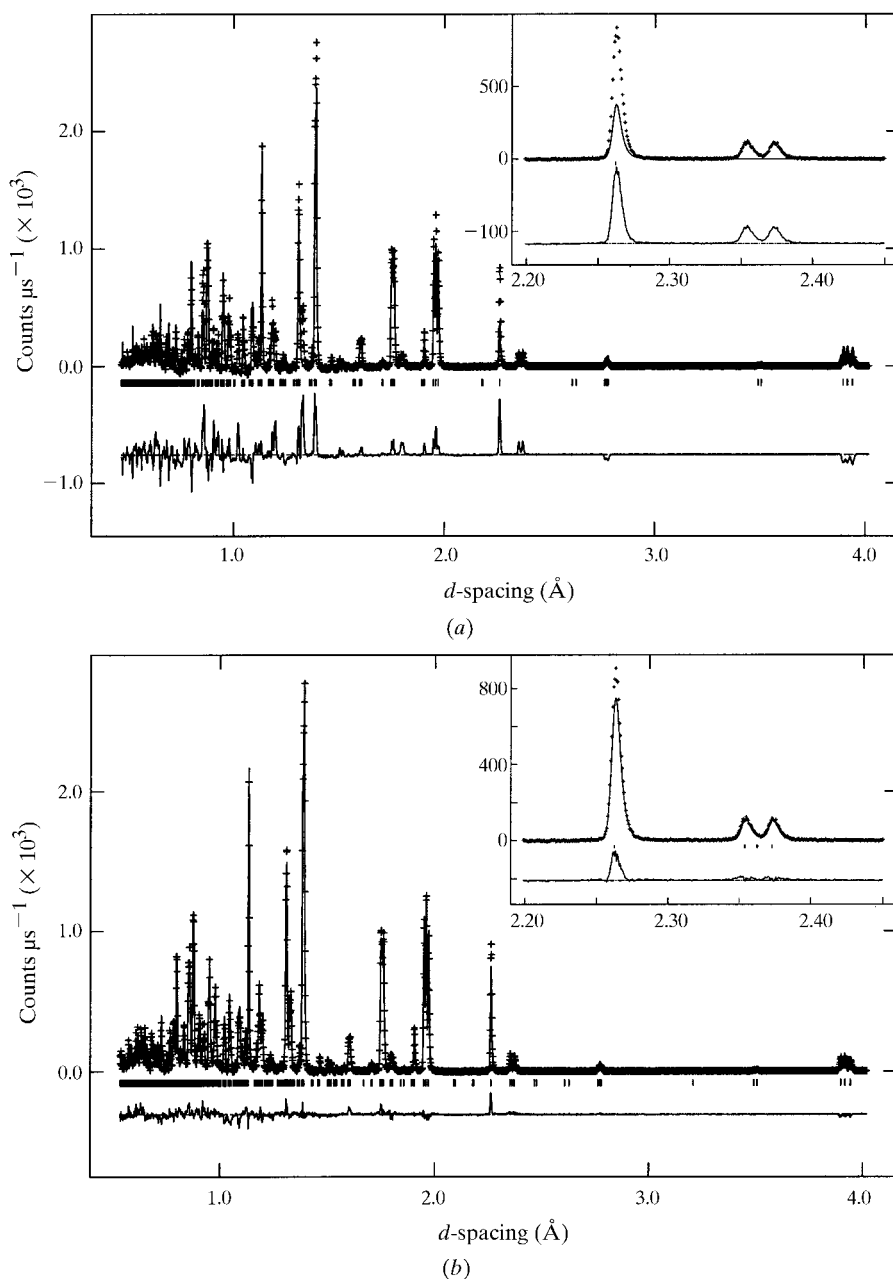


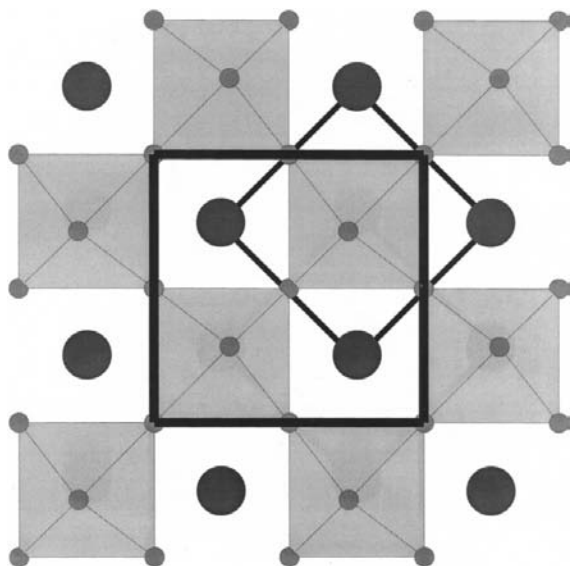
Figure 2 Refinements of $\text{Ce}_{1/3}\text{NbO}_3$ based upon (a) $Pmmm$ and (b) $P2/m$ (++) experimental data, – calculated profile). Tick marks indicate the reflection positions and the difference profile is shown at the bottom. The insets illustrate how some peaks have reflection markers in the $P2/m$ model which are not accounted for by the $Pmmm$ model.

Table 2

 Fractional atomic coordinates and equivalent isotropic displacement parameters (\AA^2) for $\text{Ce}_{1/3}\text{NbO}_3$.

	$U_{\text{eq}} = (1/3)\sum_i \sum_j U^{ij} a^i a^j \mathbf{a}_i \cdot \mathbf{a}_j$			
	<i>x</i>	<i>y</i>	<i>z</i>	U_{eq}
Ce	0.255 (2)	0	0.756 (2)	0.0120 (6)
Nb	0.2458 (8)	0.2613 (2)	0.2527 (7)	0.01624
O1	0.271 (1)	1/2	0.286 (1)	0.02033
O2	0.224 (1)	0	0.212 (1)	0.01881
O3	1/2	0.2059 (5)	1/2	0.0154
O4	0	0.223 (1)	1/2	0.01346
O5	1/2	0.242 (1)	0	0.02488
O6	0	0.2626 (5)	0	0.02277

While refinement of $\text{Ce}_{1/3}\text{NbO}_3$ with isotropic displacement parameters fit the observed profile well ($R_p = 0.0467$, $R_{\text{wp}} = 0.0677$ and $\chi^2 = 3.593$ for 37 parameters), introduction of anisotropic displacement parameters improved the fit (Table 1). In the case of Ce, the U^{11} parameter attained a value of -0.004 (4). As this value was not physical, the model was again refined, this time with isotropic temperature factors for Ce and anisotropic temperature factors for all other atoms. The displacement parameters for the O atoms from this refinement are generally strongly anisotropic, reflecting the considerable atomic scale disorder due to the partial occupancy of the Ce site. For instance, the anisotropy of the O1 atoms can be associated with the empty Ce sites in the layer at $y = \frac{1}{2}$ and the O2 atoms with the $2/3$ occupancy of the Ce site in the layer at $y = 0$. Generally, the U^{ij} parameters of oxygen are large perpendicular to the Nb–O bonds and relatively small in the direction of those bonds (Fig. 4). This anisotropy is

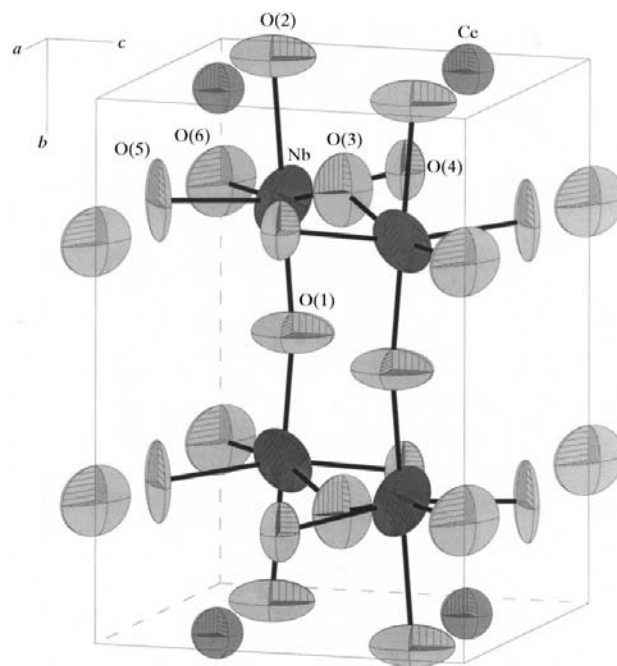

Figure 3

[010] projection of the relationship between the small orthorhombic cell and the large monoclinic cell. The orthorhombic cell is surrounded by thin lines, while the monoclinic cell is surrounded by heavy lines. The large circles indicate cerium, small circles are oxygen and niobium sites within the octahedra.

consistent with the view that only an average tilt pattern is described by the structure model. While splitting of the oxygen atomic positions was attempted, in no case was there a significant improvement of the fit. A model containing cerium at the $y = \frac{1}{2}$ layer was also examined. The refined occupancy factor for this site was zero within experimental uncertainty. This supports the segregation of Ce atoms into alternate layers.

The possible range of Ce-site occupation was determined to be 0.33–0.37 Ce atoms per formula unit by Abakumov *et al.* (1995). As a range of values for the occupation of this site was observed, refinement of this parameter was attempted in this work. Refinement of the Ce-site occupancy at $y = 0$ resulted in a slightly lower χ^2 value (2.521) for the formula $\text{Ce}_{0.37}\text{NbO}_3$. As the sample was prepared at high temperature in air, and Nb is expected to be in the 5+ oxidation state, the additional 0.04 Ce cations could only occur in conjunction with an excess of oxygen. However, all the oxygen sites in the model are fully occupied and the refinement does not suggest the presence of oxygen in additional sites. As further evidence to support a stoichiometry of $\text{Ce}_{0.37}\text{NbO}_3$ was not available and only a minor improvement of the profile fit was obtained, the occupancy was held at $\text{Ce}_{1/3}\text{NbO}_3$ in the final refinement.

Although reasonable values were obtained for the refinement in $P2/m$, attempts were made to improve the fit by using the $P2$ and Pm subgroups of $P2/m$. The refinement statistics improved only slightly ($\chi^2 = 3.511$ and 3.536, respectively) over the profile fit of $P2/m$ ($\chi^2 = 3.593$ with isotropic displacement parameters). Moreover, owing to the increase in the overall number of parameters the refinements in $P2$ and Pm were less stable than in $P2/m$. Results of the refinement in


Figure 4

The unit cell of $\text{Ce}_{1/3}\text{NbO}_3$. The thermal ellipsoids are drawn at 99% probability.

Table 3
Anisotropic displacement parameters (\AA^2) for $\text{Ce}_{1/3}\text{NbO}_3$.

	U^{11}	U^{22}	U^{33}	U^{12}	U^{13}	U^{23}
Ce	0.0120 (6)	0.0120 (6)	0.0120 (6)	0.00	0.00	0.00
Nb	0.0131 (3)	0.0206 (7)	0.015 (3)	0.007 (1)	-0.0008 (5)	-0.003 (1)
O1	0.023 (4)	0.008 (1)	0.030 (4)	0.00	-0.001 (2)	0.00
O2	0.017 (3)	0.009 (1)	0.031 (4)	0.00	-0.003 (2)	0.00
O3	0.008 (4)	0.023 (2)	0.015 (4)	0.00	-0.008 (2)	0.00
O4	0.012 (4)	0.024 (3)	0.005 (3)	0.00	0.005 (2)	0.00
O5	0.033 (5)	0.028 (4)	0.014 (4)	0.00	0.013 (2)	0.00
O6	0.033 (5)	0.023 (2)	0.012 (4)	0.00	-0.013 (2)	0.00

Table 4
Bond angles ($^\circ$) for $\text{Ce}_{1/3}\text{NbO}_3$.

$\text{O2}-\text{Ce}-\text{O2}^{\text{i}}$	172.6 (6)	$\text{Nb}-\text{O1}-\text{Nb}^{\text{vi}}$	166.0 (4)
$\text{O2}^{\text{ii}}-\text{Ce}-\text{O2}^{\text{iii}}$	172.7 (6)	$\text{Nb}-\text{O2}-\text{Nb}^{\text{vii}}$	165.7 (3)
$\text{O3}-\text{Ce}-\text{O6}^{\text{iv}}$	172.7 (3)	$\text{Nb}-\text{O3}-\text{Nb}^{\text{iii}}$	154.8 (3)
$\text{O4}-\text{Ce}-\text{O5}^{\text{v}}$	176.4 (6)	$\text{Nb}-\text{O4}-\text{Nb}^{\text{ii}}$	162.3 (5)
$\text{O1}-\text{Nb}-\text{O2}$	179.1 (5)	$\text{Nb}-\text{O5}-\text{Nb}^{\text{viii}}$	171.2 (6)
$\text{O3}-\text{Nb}-\text{O6}$	167.6 (2)	$\text{Nb}-\text{O6}-\text{Nb}^{\text{ix}}$	179.4 (3)
$\text{O4}-\text{Nb}-\text{O5}$	166.8 (2)		

Symmetry codes: (i) $x, y, 1+z$; (ii) $-x, y, 1-z$; (iii) $1-x, y, 1-z$; (iv) $-x, -y, 1-z$; (v) $1-x, -y, 1-z$; (vi) $x, 1-y, z$; (vii) $x, -y, z$; (viii) $1-x, y, -z$; (ix) $-x, y, -z$.

$P2/m$, using anisotropic displacement parameters, were therefore taken as the appropriate structure solution. The final results are presented in Tables 1, 2 and 3, and the observed, calculated and difference profiles are shown in Fig. 2(b).¹

5. Discussion

The well known perovskite (ABO_3) structure is based on a corner-sharing BO_6 octahedral sublattice. The A cations fill the space between the octahedra and sit in a 12-fold coordinated site in the ideal structure with cubic symmetry, $Pm\bar{3}m$. This symmetry can be broken by distortions resulting from the ratio of the A cation to B cation size (the Goldschmidt tolerance factor) or various electronic effects. Distortions from the ideal cubic structure are common in perovskite compounds and symmetries from triclinic to cubic have been identified (Woodward, 1997a). Despite the lower symmetry, a strong pseudocubic character is always present (the electron diffraction pattern in Fig. 1 illustrates that the β angle is close to 90°). As a result, the pseudocubic cell can be used as a basis for comparing perovskite compounds.

Glazer has developed a standard notation to describe octahedral tilting relative to a pseudocubic perovskite cell (Glazer, 1972). In monoclinic $\text{Ce}_{1/3}\text{NbO}_3$ (Fig. 5), the octahedra are tilted relative to the ideal cubic framework. The tilting is evident from the $\text{Nb}-\text{O}-\text{Nb}$ bond angles shown in Table 4. The angles differ significantly from the 180° observed

¹Supplementary data for this paper are available from the IUCr electronic archives (Reference: BR0090). Services for accessing these data are described at the back of the journal.

in the $Pmmm$ model. In Glazer's notation this structure would follow the tilt system $a^0b^-c^-$, which indicates that there is tilting along two of three crystal axes of the pseudocubic cell. Other compounds which are known with this tilt system include $\text{Ba}(\text{Pb}_{1-x}\text{Bi}_x)\text{O}_3$ ($0.2 \geq x \geq 0$) and BaPbO_3 (in the $I2/m$ space group; Woodward, 1997b). It is interesting to note that $C2/m$ (the standard space-group setting for $I2/m$) has been derived independently for this tilt system by a group-theoretical analysis of the symmetry

(Howard & Stokes, 1998). However, ordering of the cerium into alternate (010) layers requires the use of the lower-symmetry ($P2/m$) space group setting for $\text{Ce}_{1/3}\text{NbO}_3$.

The Goldschmidt tolerance factor can be used as a predictor for the occurrence of octahedral tilting in ABX_3 perovskites (Goodenough & Zhou, 1998). The tolerance factor from experimentally derived bond lengths for $\text{Ce}_{1/3}\text{NbO}_3$ is 0.969. This is higher than the value from the sum of the ionic radii (0.956), using the tabulated ionic radii of Shannon (1976) with coordination numbers 12 for Ce^{3+} , 6 for Nb^{5+} and 2 for O^{2-} . This is not surprising as one might expect the oxygen to relax (on average) away from the cation-deficient cerium site, thereby increasing the $A-X$ bond length and increasing the tolerance factor closer to the ideal value of 1.0.

Interestingly, a bond-valence analysis suggests that a distortion of the $\text{Ce}-\text{O}$ coordination sphere is essential for

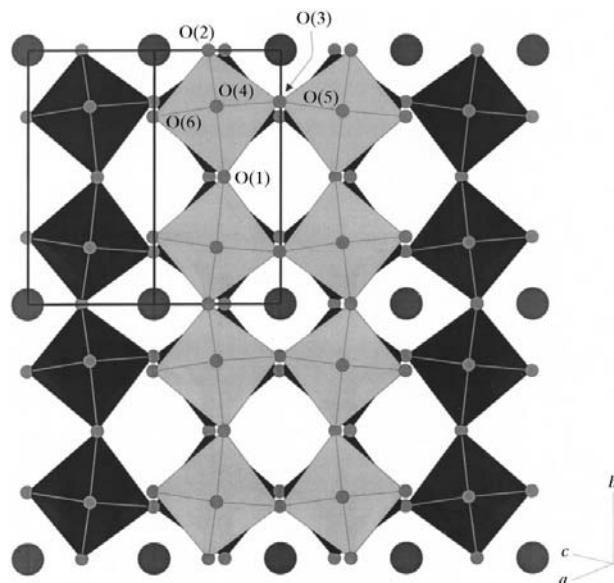


Figure 5
View of $\text{Ce}_{1/3}\text{NbO}_3$, which illustrates tilting of NbO_6 octahedra as well as ordering of Ce atoms in successive layers along the b axis. The view is along the $[10\bar{1}]$ face and the unit cell is drawn at the top left of the figure. Large circles indicate cerium, small circles are oxygen and niobium sits within the octahedra. The labeled structure axes are tilted downwards slightly with respect to the viewing direction (the c axis is pointing into the paper).

Table 5
Selected bond distances (Å) and [bond valences] in $\text{Ce}_{1/3}\text{NbO}_3$.

	O1	O2	O3	O4	O5	O6	Σ_s
Nb	1.896 (2) [1.041]	2.075 (2) [0.642]	2.003 (4) [0.780]	1.955 (4) [0.888]	1.991 (4) [0.806]	1.943 (4) [0.917]	[5.074]
Ce		2.53 (1), 2.65 (2), 3.01 (1), 2.89 (2) [0.364, 0.262, 0.098, 0.136]	2.548 (7) [0.342]	2.66 (10) [0.255]	2.70 (1) [0.230]	2.846 (6) [0.153]	[2.820]
Σ_s	[2.082]	[1.857]	[2.016]	[2.116]	[1.919]	[2.038]	

The Ce–O contributions to the bond-valence sums for O2, O3, O4, O5 and O6 have all been multiplied by a factor of 2/3 before summation, owing to the 2/3 occupation of the Ce site.

cerium. Bond-valence sums (Brown & Altermatt, 1985) were calculated using the program Valist (Wills & Brown, 1999) for the Nb and Ce coordination polyhedra and are presented in Table 5. Using the average experimental Ce–O bond length (2.710 Å), the bond-valence sum of cerium is calculated to be 2.649, which is significantly less than the value of 2.820 calculated directly from the individual experimental bond lengths. This may suggest that the bond-valence requirements of Ce are in a large part responsible for the octahedral tilting, which drives the distortion to monoclinic symmetry.

The niobium coordination environment is composed of one short (1.896), four intermediate (1.943–2.003) and one long (2.075) bond to oxygen (Table 5). The shortest bond is between Nb and O1, which is the O atom in the (010) layer without cerium. This result follows logically from bond-valence arguments. Simply put, as the bond valence of O1 is only shared by two Nb atoms, the Nb–O1 bond length is short. As Table 5 indicates, O atoms which are bound to more cations have smaller bond valences and greater bond lengths. In addition, the out-of-center distortion is a common one for Nb^{5+} cations in octahedral coordination. A second-order Jahn–Teller distortion can occur when the vacant *d* band approaches degeneracy with the Fermi level (Kunz & Brown, 1995).

Comparison of the previous results for $\text{La}_{0.38}\text{NbO}_3$, solved using X-ray powder diffraction in *Pm3m* by Abakumov *et al.* (1995), reveal important differences. The *Pm3m* symmetry allows niobium to shift towards the layer unoccupied by lanthanum, but restricts displacements parallel to that layer. Moreover, the octahedral tilting which is found in the *P2/m* model is not possible in the *Pm3m* model. This suggests that in the case of $\text{Ce}_{1/3}\text{NbO}_3$ the lack of octahedral tilting in the *Pm3m* model prevents the lattice from achieving the minimum stress. Given the inability of X-ray diffraction to

detect the distortion present in the *P2/m* model, it is likely that a similar situation exists for the other $\text{Ln}_{1/3}\text{NbO}_3$ and $\text{Ln}_{1/3}\text{TaO}_3$ materials which have been described previously in *Pm3m*.

We thank Simine Short of the IPNS facility at Argonne National Laboratory for obtaining the powder neutron data. We thank as well the Natural Sciences and Engineering Research Council of Canada for support of this work through a research grant to J. E. Greedan.

References

- Abakumov, A. M., Shpanchenko, R. V. & Antipov, E. V. (1995). *Mater. Res. Bull.* **30**, 97–103.
- Brown, I. D. & Altermatt, D. (1985). *Acta Cryst.* **B41**, 244–247.
- Glazer, A. M. (1972). *Acta Cryst.* **B28**, 3384–3392.
- Goodenough, J. B. & Zhou, J. S. (1998). *Chem. Mater.* **10**, 2980–2993.
- Hewat, A. W. (1979). *Acta Cryst.* **A35**, 248.
- Howard, C. J. & Stokes, H. T. (1998). *Acta Cryst.* **B54**, 782–789.
- Iyer, P. N. & Smith, A. J. (1967). *Acta Cryst.* **23**, 740–746.
- Jorgensen, J. D., Faber, J. Jr, Carpenter, J. M., Crawford, R. K., Haumann, J. R., Hitterman, R. L., Kleb, R., Ostrowski, G. E., Rotella, F. J. & Worlton, T. G. (1989). *J. Appl. Cryst.* **22**, 321–333.
- Kunz, M. & Brown, I. D. (1995). *J. Solid State Chem.* **115**, 395–406.
- Larson, A. C. & Von Dreele, R. B. (1986). Los Alamos National Laboratory Report, LA-UR-86-748. Los Alamos, New Mexico, USA.
- Orgaz, E. & Huanosta, A. (1992). *J. Solid State Chem.* **97**, 65–73.
- Shannon, R. D. (1976). *Acta Cryst.* **A32**, 751–767.
- Torardi, C. C., Brixner, L. H. & Foris, C. M. (1985). *J. Solid State Chem.* **58**, 204–210.
- Von Dreele, R. B., Jorgensen, J. D. & Windsor, C. G. (1982). *J. Appl. Cryst.* **15**, 581–589.
- Wills, A. S. & Brown, I. D. (1999). Valist, CEA, France. Program available from author at willsas@netscape.net.
- Woodward, P. M. (1997a). *Acta Cryst.* **B53**, 32–43.
- Woodward, P. M. (1997b). *Acta Cryst.* **B53**, 44–66.